A simple method for the analysis of neutron resonance capture spectra

Martijn C. Clarijs,[a] Victor R. Bom, and Carel W. E. van Eijk
Radiation, Detection and Medical Imaging, Delft University of Technology, Mekelweg 15, 2629 JB Delft, The Netherlands

(Received 7 November 2008; accepted 2 February 2009; published online 20 March 2009)

Neutron resonance capture analysis (NRCA) is a method used to determine the bulk composition of various kinds of objects and materials. It is based on analyzing direct capture resonance peaks. However, the analysis is complicated by scattering followed by capture effects in the object itself. These effects depend on the object's shape and size. In this paper the new Delft elemental analysis program (DEAP) is presented which can automatically and quickly analyze multiple NRCA spectra in a practical and simple way, yielding the elemental bulk composition of an object, largely independent of its shape and size. The DEAP method is demonstrated with data obtained with a Roman bronze water tap excavated in Nijmegen (The Netherlands). DEAP will also be used in the framework of the Ancient Charm project as data analysis program for neutron resonance capture imaging (NRCI) experiments. NRCI provides three-dimensional visualization and quantification of the internal structure of archaeological objects by performing scanning measurements with narrowly collimated neutron beams on archaeological objects in computed tomography based experimental setups. The large amounts (hundreds to thousands) of spectra produced during a NRCI experiment can automatically and quickly be analyzed by DEAP. © *2009 American Institute of Physics*. [DOI: 10.1063/1.3094010]

I. INTRODUCTION

Neutron resonance capture analysis (NRCA) is based on the existence of resonances in neutron capture cross sections in the epithermal energy range for almost all nuclei. As these resonances are characteristic for each element, their observation and quantitative analysis provide information about the occurrence and concentration of the elements in an object.

NRCA has been developed at the GELINA pulsed neutron facility of the European Commission (EC) Joint Research Centre, Institute of Reference Materials and Measurements (IRMM) in Geel (Belgium), starting in 2000 as a joint project between that institute and Delft University of Technology (The Netherlands). It has been applied in a series of experiments on archaeological bronzes.[1–6] The elemental composition of such artifacts, including trace elements, may be helpful in the determination not only of its origin and that of its raw materials (e.g., metal ore), but also of the way they were produced, thus helping to learn more about trade routes and production methods in prehistoric times. In addition information about the authenticity of objects can, under suitable conditions, be obtained as has been shown for a series of Etruscan statuettes.[3]

NRCA can be applied to detect most of the medium and heavy weight elements as these are characterized by neutron resonance energies suitable for analysis roughly in the range of 1 eV–10 keV. Energy information for resonances in the neutron capture process is obtained by means of time-of-flight (TOF) measurement over a well defined neutron-path length. Most of the lighter elements and some nuclides with or close to double magic numbers have neutron resonances at energies too high to be conveniently measured with the TOF method. NRCA provides bulk elemental composition because of the large penetration depth of neutrons in dense (high Z) materials, as opposed to x-ray fluorescence techniques and particle induced x-ray emission that yield information about the composition of the "skin" of an object as x-rays are strongly absorbed in high Z materials. Since bulk and skin compositions of an object can differ significantly due to degradation processes at the surface, e.g., oxidation, NRCA offers a clear advantage to the archaeologist. At present, NRCA is being further developed in the framework of the Ancient Charm[7] project to provide visualization and quantification of the internal structure of archaeological objects by means of three-dimensional (3D) imaging of the elemental number densities.

For NRCA we need, in addition to an advanced facility like GELINA, an advanced neutron resonance spectrum analysis code. In principle NRCA is based on direct capture of neutrons. However, capture preceded by single or multiple scattering occurs as well and this affects the spectra. Furthermore, the number of neutrons decreases with increasing depth in the sample and, due to this self-shielding effect, the spectral line shapes depend on the sample thickness.

A well-established analysis code used to determine resonance parameters and capture yields, taking into account scattering effects, self-shielding, and some other effects, is REFIT.[8] Using samples with well-defined composition and shape, the influence of scattering and self-shielding on derived resonance parameters can be controlled and/or modeled, making REFIT a valuable tool for neutron physicists to assess neutron resonance parameters for applications such as, e.g., nuclear reactor technology and nuclear shielding materials.

Whereas REFIT can straightforwardly be used to analyze the complete spectrum of samples with well-defined compo-

[a]Electronic mail: m.c.clarijs@tudelft.nl.

sition and shape, this is not *a priori* the case for archaeological objects. These may, in general, be characterized to have (partly) unknown composition, irregular shapes, and (inner) dimensions that cannot easily be modeled. Also, archaeological objects are usually thicker than those that can be manufactured comfortably thin for neutron resonance parameter studies, which implies that pronounced scattering and self-shielding complicate spectral analysis.

So far the analysis of NRCA data has been based on ratios of integrated count rates (peak areas) of two resonances from different elements.[1] Each resonance peak area is corrected for the underlying background including a shoulder due to scattering followed by capture (see Sec. IV). These ratios are calculated for both the object and a calibration sample. This gives a double ratio, and since the weight ratio for the elements in the calibration sample is accurately known, the weight ratio of these two elements in the object can be derived. It is often possible to analyze several pairs of resonances. Each pair must be corrected for resonance self-shielding, which is different for different resonances and which depends on the thickness of the sample. This dependence makes it possible to derive, under suitable conditions, an effective thickness of the sample. Good results have been obtained with this double-ratio method and consistency with neutron diffraction measurements has been found.[9]

An analysis method which performs the steps as described for the double-ratio method in a fully automated way in one go and which is only slightly dependent on object shape and size would therefore be a clear asset to those studying archaeological objects. In addition to this, the anticipated use of analysis software mainly by archaeologists rather than neutron physicists implies that ease of use and speed of analysis are becoming even more essential parameters that decide whether such a program will actually be suitable for relatively inexperienced users. For the archaeologist, the most important information derived from NRCA is the elemental composition. Based on the above arguments, we have developed a software package implementing an analysis method for the elemental composition of an arbitrary object. In principle, the new code, Delft elemental analysis program (DEAP), uses the above double-ratio approach by comparing a (small) set of resonances of the object with those of a calibration sample, but with corrections for self-shielding and scattering followed by capture included and with a fully automated fitting procedure.

II. NEUTRON RESONANCES AND EXPERIMENTAL TECHNIQUES

Neutron capture by a nucleus with atomic and mass numbers (Z,A) leads to a compound nucleus $(Z,A+1)$ with the capture state at an excitation energy roughly equal to the neutron binding of about 8 MeV. This energy is released by the emission of several (2–6) prompt high energy γ-rays in cascade. The detection of these γ-rays provides the timing signal for the capture event.

Experiments were performed at the GELINA TOF facility, which is a linear electron accelerator with a maximum electron energy of 150 MeV and a maximum beam power of

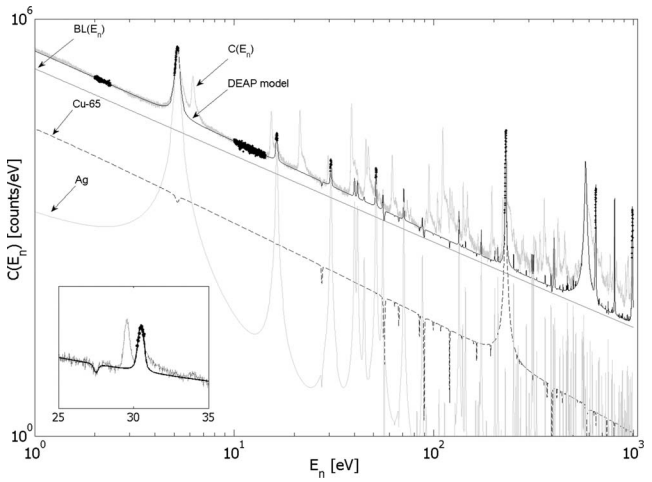

FIG. 1. Comparison between recorded dead-time corrected capture counts $C(E_n)$ for the Nijmegen water tap and DEAP analysis for Cu and Ag, with separate contributions to $C(E_n)$ from Cu-65 and Ag and baseline intensity $\mathrm{BL}(E_n)$. Only bold data points have been selected for analysis. The inset shows data and DEAP model for the Ag resonance at 30.4 eV. In the DEAP model the use of cadmium as an overlap filter is taken into account. This is clear from the small dips in the DEAP model line in the figure.

10 kW with a pulse rate of up to 800 Hz. The pulse width after the bunching magnet is as short as 1 ns. Neutrons are produced when the electrons hit a uranium target. To enhance the neutron intensity in the low energy domain, two water-filled Be containers (4 cm thick) serve to partially moderate the neutrons. They are placed just above and below the uranium target. The energy-dependent neutron fluence rate at a flight path length L (in meters) from the production source is in good approximation $\varphi_0(E_n)=1.6\times10^6L^{-2}E_n^{\alpha}$ $(\mathrm{s}^{-1}\,\mathrm{eV}^{-1}\,\mathrm{cm}^{-2})$ with E_n (eV) the neutron energy and[10] $\alpha=-0.89+3.27\times10^{-4}\sqrt{E_n}-2.9\times10^{-7}E_n$.

The experimental data depicted as $C(E_n)$ in Fig. 1 correspond to $L\approx12.9$ m and are taken from a NRCA measurement of the cylindrical part of a Roman water tap from the second century A.D., excavated in Nijmegen (NL), and now belonging to the collection of the Rijksmuseum van Oudheden (National Museum of Antiquities) in Leiden (NL) as published by Schut *et al.*[9] In the present paper, results from Schut *et al.*[9] will be compared with those from the DEAP analysis method. Results from a second study employing the DEAP analysis method will also be published.[11]

In the NRCA setup, two C_6D_6-scintillation detectors (with diameter of 12.5 cm and thickness of 7.5 cm) were installed opposite to each other on either side of the neutron beam, with their front sides 7 cm from the center of the 7 cm diameter circular beam, i.e., outside the incoming beam but close enough to the object to maximize the solid angle for detection. The C_6D_6 scintillators detect the γ-radiation emitted after neutron capture. They are very insensitive to neutrons. A disk of lead (15 mm thick) was placed in the beam just outside the neutron production hall as a filter to stop bremsstrahlung γ-ray flashes, which would otherwise saturate the detectors for several microseconds. In a second experiment the lead filter was replaced by a bismuth filter (15 mm thick) to determine the amount of lead in the Nijmegen water tap. In addition, a cadmium sheet (0.75 mm

thick) was placed at this position to remove neutrons with energies below 0.7 eV from the beam in order to avoid overlap of consecutive beam pulses. The TOF is directly derived from the time difference between the moments of the C_6D_6 detector response and initial neutron production pulse. The recorded TOF spectrum is related to the energy spectrum by

$$E_n = \left(72.798\frac{L}{T+T_0}\right)^2 \tag{1}$$

with T the TOF in microseconds and T_0 a constant representing a small time offset within the experimental system. Already during data taking, resonance peaks can be recognized, thus providing a quick and qualitative analysis of the elemental composition.

III. RELATION BETWEEN OBJECT COMPOSITION AND NRCA SPECTRA

Assume an object with a composition consisting of i homogeneously mixed elements and thickness d (cm) in the direction of the incoming neutron beam. The elemental composition is derived from the experimental dead-time corrected capture count rate following the expressions below.

The theoretical direct capture (DC) yield per neutron through a homogeneous layer with thickness d can be expressed[12] by

$$Y_{\mathrm{DC}}(E_n)|_d = \left\{1-\exp\left[-\left(\sum_i N_i\sigma_{t,i}^D(E_n)\right)d\right]\right\} \times \frac{\Sigma_i N_i\sigma_{c,i}^D(E_n)}{\Sigma_i N_i\sigma_{t,i}^D(E_n)} \tag{2}$$

with N_i (atoms cm^{-3}) the elemental number density and $\sigma_{t,i}^D$ and $\sigma_{c,i}^D$ (barn), respectively, the Doppler-broadened microscopic total and capture cross sections for element i. The total cross section also contains potential scattering.

N_i is lower than the pure elemental number density due to the presence of other elements in the object, which is accounted for in the proposed analysis method by a density correction factor f_i:

$$N_i = f_i\frac{N_a}{M_i}\rho_i \tag{3}$$

with N_a as Avogadro's number, M_i ($\mathrm{g\,mol}^{-1}$) the atomic mass, and ρ_i ($\mathrm{g\,cm}^{-3}$) the mass density of the pure element.

The theoretical total capture (TC) yield per neutron for a layer of thickness d also contains terms related to scattering followed by capture, that is,

$$Y_{\mathrm{TC}}(E_n)|_d = Y_{\mathrm{DC}}(E_n)|_d + Y_{\mathrm{SC}}(E_n)|_d, \tag{4}$$

where SC stands for all possible scattering followed by capture events. This will be treated in Sec. IV.

To compare the theoretical yield with experimental data, it is necessary to modify the theoretical yield by multiplying it with the neutron beam fluence rate $\varphi(E_n')$ and with the relative efficiency $\varepsilon_{c,\mathrm{rel}}(E_n')$ for detecting capture events. The next step is to convolute this expression with the neutron energy resolution function $R(E_n,E_n')$, expressing the probability that a neutron with energy E_n' will result in a capture event recorded at a TOF corresponding to E_n. This leads to the following yield expression in units (s^{-1}) to be fitted to the data:

$$\Delta Y_{\mathrm{TC}}(E_n) = K_1 R(E_n,E_n') \otimes \{\varepsilon_{c,\mathrm{rel}}(E_n')\varphi(E_n')Y_{\mathrm{TC}}(N_i,E_n',d)\}\Delta E_n'\Delta O. \tag{5}$$

This is the yield of capture events in a small energy interval ΔE for a narrow beam entering an object through an area ΔO. It is useful for neutron resonance capture imaging (NRCI) experiments in which narrow beams are used.

We use calibration measurements to determine $\varepsilon_{c,\mathrm{rel}}(E_n')$ at resonance energies, see Sec. VI A. Since in the general case the absolute neutron flux is not necessarily known and only the energy dependence can be accurately determined, the constant factor K_1 is used in the analysis to normalize the theoretical yields into experimental yields.

In the case of a wide beam, as used for NRCA with an irregular shaped artifact, Eq. (5) must be integrated over the shape of this object. In principle the neutron flux may vary across the beam, making the integration even more complex. The total yield of expected capture events is formally given by

$$Y_{\mathrm{TC}}(E_n) = \int_{\mathrm{object}} \Delta Y_{\mathrm{TC}}(E_n). \tag{6a}$$

This function must be fitted to the experimental yield of capture events given by

$$Y_{\mathrm{TC,exp}}(E_n) = C'(E_n) - B'(E_n). \tag{6b}$$

$C'(E_n)$ is the dead-time-corrected capture count rate and $B'(E_n)$ is the dead-time-corrected background count rate.

IV. CAPTURE AFTER SCATTERING

The analysis of NRCA spectra is based on DC of neutrons, i.e., capture events occurring in the object without previous interaction. However, in general, the analysis is complicated by neutron scattering and subsequent capture in the object (SC). Capture may take place after one (single), two (double), or, in general, multiple scattering events, henceforth referred to as SSC, DSC, and MSC.

For neutrons with epithermal off-resonance energies, potential scattering is the dominant interaction process. If potential scattering is followed by resonance capture (both in the object), SC events are recorded with energies just above the resonance energy: The initial neutron energy is decreased during the scattering event, resulting in a scattered neutron that has an energy that matches the high resonance capture probability, but the recorded TOF for this event remains virtually unaltered. The resulting SC spectra or "shoulder" on the high energy side of the capture peaks can clearly be seen in Fig. 2(a)–2(c) for the ^{65}Cu resonance at 230 eV. The different shapes of the SC spectra can be understood from Secs. IV A–IV C.

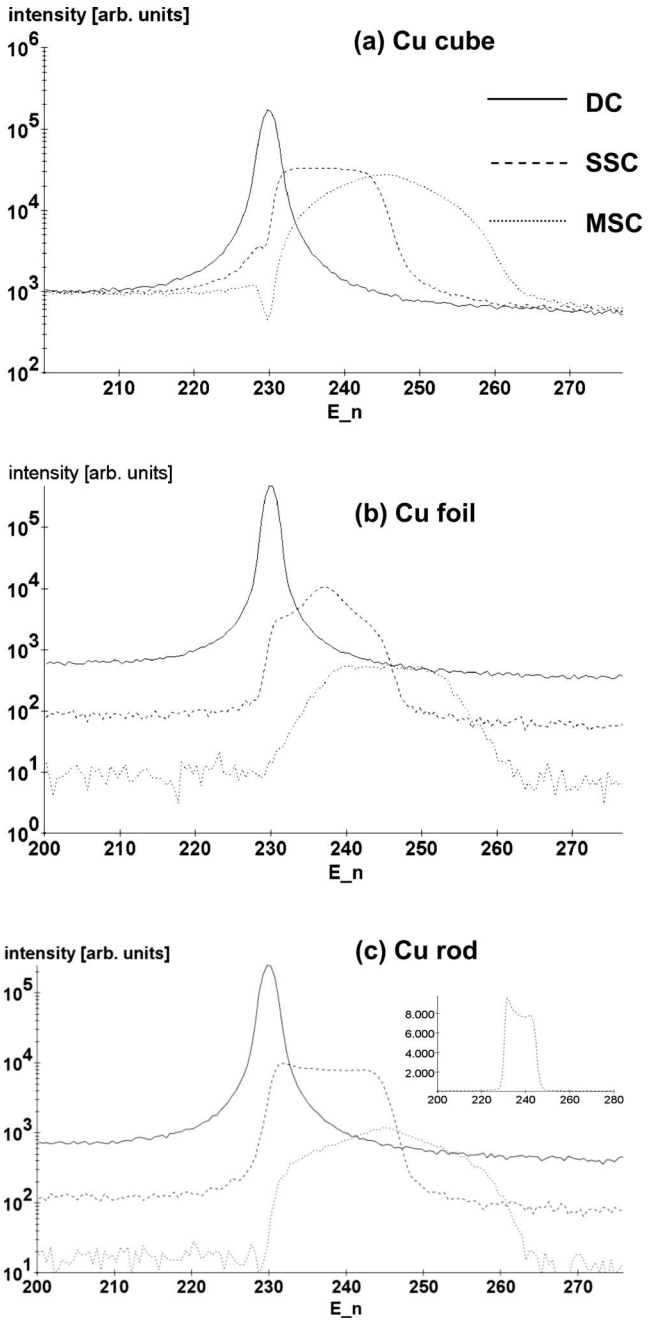

FIG. 2. Results of GEANT4 simulated neutron interactions for initial neutron energies around the ^{65}Cu resonance at 230 eV, for a big Cu cube ($10\times10\times10$ mm^3), a thin Cu foil ($40\times40\times1$ mm^3) perpendicular to, and a thin Cu rod ($\oslash$=1 mm and height=40 mm) aligned with the incoming neutron beam ($\oslash$=5 mm, GELINA fluence rate), respectively. DC, SSC, and DSC intensities represent the number of neutrons that interacted via such events (γ absorption in object and detection efficiency were not simulated) and are illustrated by full, dashed, and dotted curves, respectively.

A. Neutron scattering

In the scattering process on a nucleus with mass number $A \gg 1$, the neutron loses energy as recoil energy E_{rec} to the scattering nucleus,

$$E_{\mathrm{rec}} = (1-\cos\theta)E_{n,0}\frac{2M/m_n}{(M/m_n+1)^2} \tag{7}$$

with $E_{n,0}$ the neutron energy before scattering and M and m_n the nuclear and neutron mass, respectively. In approximation

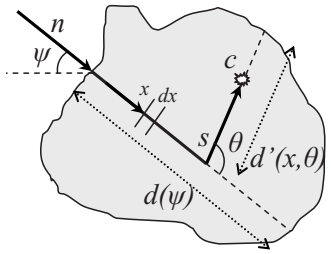

FIG. 3. Two-dimensional geometry for SC in an irregularly shaped object with indicated positions of neutron scattering (S) and subsequent capture (C).

$M/m_n=A$. The angle θ is the scattering angle in the center of mass system, varying from zero to 180°. For $A \gg 1$ the scattering angle in the laboratory system is in good approximation equal to the angle in the center of mass system. The maximum energy transfer $E_{\mathrm{rec,max}}$ occurs in a head-on collision and is in good approximation:[13]

$$E_{\mathrm{rec,max}} = \frac{4A}{(A+1)^2}E_{n,0}. \tag{8}$$

Thus, a neutron with energy $E_{n,0}$ has, after a single scattering event, the energy $E_{n,1}$ in the range of $E_{n,0}-E_{\mathrm{rec,max}} < E_{n,1} < E_{n,0}$.

At low neutron energies, scattering is mainly an s-wave process and thus it is isotropic. It can then be shown that all recoil energies are equally possible.[13] The probability for the neutron with energy $E_{n,0}$ to be scattered to an energy $E_{n,1}$ is given by

$$P_s(E_{n,0},E_{n,1}) = \frac{1}{E_{\mathrm{rec,max}}}. \tag{9}$$

Thus, the basic form of the structure due to single scattering followed by capture by a sharp resonance with central energy E_{res} is rectangular from E_{res} to $E_{\mathrm{res}}+E_{\mathrm{rec,max}}$, which is modified by twice the Doppler broadening at the scattering and capture nuclei, by energy dependence of the neutron flux, and by the beam resolution function.[14]

Figure 3 illustrates the geometry for SSC in an arbitrarily shaped object. Along the path of the incoming beam, the neutron is scattered in an interval Δx at a distance x over an angle θ into a solid angle $\Delta\Omega$. Thereafter the neutron can be captured along the new direction over distance d' inside the object. That is,

$$\begin{aligned}\Delta y_{\mathrm{SSC}}(E_{n,0},E_{n,1},x,\theta)\Delta E_n\Delta x\Delta\Omega &= \Delta E_n[\exp\{-N\sigma_t^D(E_{n,0})x\}N\sigma_n^D(E_{n,0})\Delta x] \\ &\times\{[1-\exp\{-N\sigma_t^D(E_{n,1})d'(x,\theta)\}] \\ &\times[\sigma_c^D(E_{n,1})/\sigma_t^D(E_{n,1})]\Delta\Omega\}.\end{aligned} \tag{10}$$

Again σ_t^D and σ_n^D are the Doppler-broadened microscopic total and scattering cross sections.

For a plate Eq. (10) can be integrated to obtain the SSC yield $Y_{\mathrm{SSC}}^{\mathrm{theor}}(E_{n,0},E_{n,1})$, see Moxon *et al.*[8] and Larson *et al.*[15] In the case of an irregularly shaped object, $Y_{\mathrm{SSC}}^{\mathrm{theor}}(E_{n,0},E_{n,1})$ can only be obtained by numerical calculations or Monte Carlo methods.

Calculations for double and multiple scattering followed by capture are even more complicated. However, the influence of these events on the resonance spectra is rather limited. Consequently, rough estimations suffice in most cases.

We have therefore adopted an analysis approach that is based on avoiding SC as much as possible. This is discussed in Sec. VI A.

B. Simulations of SC

In order to better understand the SC process we have performed GEANT4 (Ref. 16) simulations of neutron interactions in three different copper object shapes. Figures 2(a)–2(c) show the results for a big copper cube, a thin copper foil perpendicular to, and a thin copper rod aligned with the incoming neutron beam direction. For the ^{65}Cu resonance at 230 eV, $E_{\mathrm{rec,max}}$ amounts to about 14 eV and so the structured SSC spectrum energy range is roughly $[E_{n,0}-E_{\mathrm{rec,max}},E_{n,0}]=230-244$ eV. Likewise, the DSC energy range is roughly $[E_{n,0}-2E_{\mathrm{rec,max}},E_{n,0}]=230-258$ eV. These ranges can be seen in Fig. 2(a)–2(c).

In the case of the Cu cube, the neutron beam was not incident on the cube outer surface but the starting position for all neutrons was the cube center. After a scattering event has occurred, the cube dimension in the direction of the scattered neutron is large (compared to the neutron mean free path length) for all θ as the neutron is surrounded by a bulk Cu medium. This means that the probability for subsequent capture is virtually independent of θ. As a consequence, similar to $P_s(E_{n,0},E_{n,1})$, the probability $P_{\mathrm{SSC}}(E_{n,0},E_{n,1})$ for SSC is in good approximation independent of E_n for $E_{n,0}-E_{\mathrm{rec,max}}<E_n<E_{n,0}$. This explains the flat part of the SSC spectrum between 230 and 244 eV. Near the low and high energy edges of this range, DC and DSC become competing processes, which explains the lower probability for SSC. The high relative intensities of SSC and DSC show that a lot of capture events occur at positions outside the initial beam direction.

In the thin Cu foil, SSC events can only take place if neutrons are scattered at approximately 90°. Neutrons scattered at other angles have a high probability of escaping the foil without being captured. The scattering angle of 90° corresponds to an energy transfer of $\frac{1}{2}E_{\mathrm{rec,max}}$, which explains the maximum at 237 eV in the SSC spectrum. Likewise, SSC events in the thin Cu rod predominantly occur at scattering angles of 0° and 180°, with corresponding energy transfers of about 0 and 14 eV, respectively. This explains the increased intensities in the SSC spectrum at the low and high energy edges.

The shapes of the spectra for DSC events are more complicated but roughly follow from convolution of the respective SSC spectra with themselves. Convolution of an approximately rectangularly shaped spectrum with itself results in a triangularly shaped spectrum.

Whereas potential scattering followed by capture causes SC structures at energies above the resonance peak, resonance scattering followed by capture adds to the recorded intensity in the resonance peak itself. The intensity of this effect depends on the ratio of scattering to capture cross sections around the resonance energy. If this ratio is large, resonance scattering followed by capture may significantly complicate the analysis. Therefore only those resonances are suitable in the analysis for which capture is the dominant process, as discussed in Sec. V.

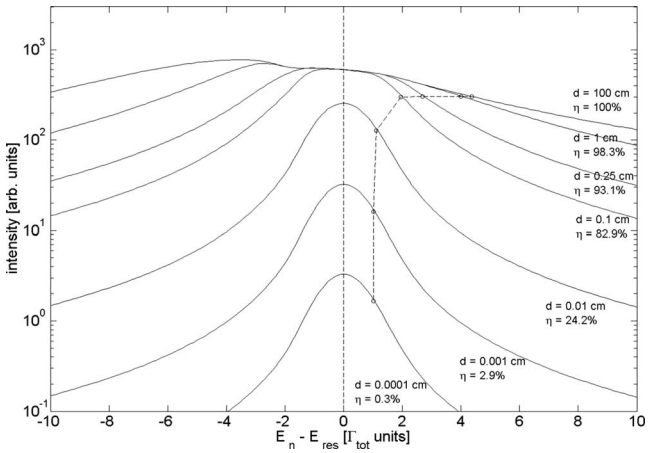

FIG. 4. $Y_{\mathrm{DC}}(E_{\mathrm{res}})$ resonance peak shapes for ^{63}Cu resonance at 579 eV calculated for various pure Cu thicknesses d (cm), as a function of E_n relative to E_{res} in units of the total neutron width Γ_{tot}. Increasing d values and corresponding self-shielding η are indicated in the figure. The joined points connect d values at half-width half maximum and illustrate the deviation from linear behavior as self-shielding sets in.

C. Total versus direct capture

From these examples it is clear that the shape and intensity of the SC spectrum depend not only on object material, size, and shape but also on the direction of the incoming neutron beam. The SC spectrum extends under the DC peak and, as a result, $Y_{\mathrm{TC,exp}}(E_n)$ may be significantly larger than $Y_{\mathrm{DC,exp}}(E_n)$, hindering straightforward composition analysis based on the latter. Adequate correction for scattering is thus needed, but if SC cannot be accurately modeled by taking into account all the above parameters, a different analysis approach must be chosen in order to avoid unacceptable systematic errors in derived elemental number densities.

In our proposed analysis method we use the fact that, for a sufficient number of experimental resonance capture peaks, the SC contribution is very low at energies under the left (low-energy) wing of the peak, i.e., $Y_{\mathrm{TC,exp}}(E_n)\cong Y_{\mathrm{DC,exp}}(E_n)$, as discussed in Sec. VI.

V. SELF-SHIELDING AND RESONANCE PEAK SHAPE

Assume an object with thickness d in the beam direction and x the neutron penetration depth within the object in the same direction. The neutron beam fluence rate at position x is given by

$$\varphi(x,E_n)=\varphi_0(E_n)\exp\left(-\sum_i N_i\sigma_{t,i}^D(E_n)\cdot x\right), \tag{11}$$

indicating that with increasing x the number of neutrons available for capture is reduced, especially for $E_n\approx E_{\mathrm{res}}$ and large cross sections. As a result, $Y_{\mathrm{DC}}(E_n)$ peak shapes change with increasing d, the so-called self-shielding effect, as illustrated in Fig. 4 for the ^{63}Cu resonance at 579 eV. For small

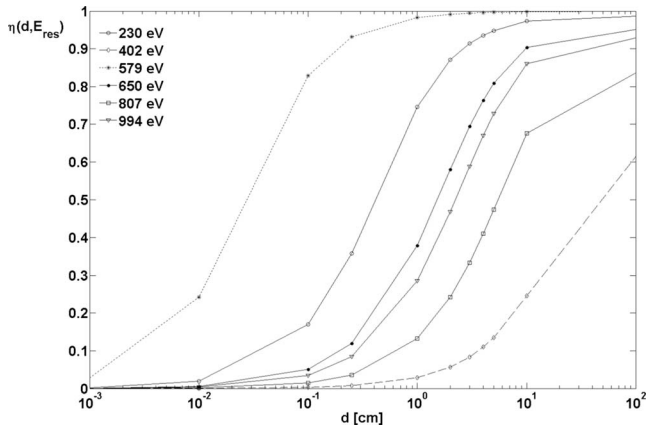

FIG. 5. Self-shielding $\eta(d,E_{\mathrm{res}})$ in a pure Cu object for different Cu resonances as a function of Cu thickness d (cm) in the direction of incoming beam.

thickness d, $Y_{\mathrm{DC}}(E_{\mathrm{res}})$ is, as expected, proportional to d. Self-shielding $\eta(d,E_n)$ can be quantified as

$$\eta(d,E_n) = 1 - \frac{Y_{\mathrm{DC}}(E_n)|_d}{d\Sigma_i N_i \sigma^0_{c,i}(E_n)}. \tag{12}$$

In first order $\eta(d,E_n)$ is given by

$$\eta(d,E_n) \cong \frac{1}{2} d \sum_i N_i \sigma^D_{t,i}. \tag{13}$$

Peak shapes clearly change with increasing d (values indicated in centimeters in Fig. 4). As an example, at the center of the strong 579 eV Cu resonance, $\eta(d,E_{\mathrm{res}})=0.24$ for $d=0.01$ cm, while $\eta(d,E_{\mathrm{res}})>0.80$ for $d>0.1$ cm. That is, with increasing d, this resonance quickly saturates at its center although capture still occurs at the wings, where self-shielding increases more slowly. In this case any useful information should be derived from resonance peak shape rather than peak intensity, which complicates analysis. Therefore the 579 eV Cu resonance is less suitable for analyzing bronzes, but it might be useful in objects with copper as a trace element.

Eventually, $Y_{\mathrm{DC,exp}}(E_{\mathrm{res},i})$ saturates and reaches an almost constant value for all resonances for $d>d_{\mathrm{lim}}$, with d_{lim} a limiting thickness value that depends on E_{res} and element abundance in the object. Almost all neutrons have then been captured or scattered out of the incoming beam before reaching the back side of the object, i.e., $\eta(d>d_{\mathrm{lim}},E_{\mathrm{res}})$ approaches 1, which makes NRCA less suitable for determining elemental compositions. One can also define d_{lim} for all resonances combined in NRCA. For bronze objects d_{lim} is in the order of a few centimeters. Figure 5 shows $\eta(d,E_{\mathrm{res}})$ in a pure Cu object for different Cu resonances as a function of d (cm) in the direction of the incoming beam.

Resonance peaks for analysis are thus to be carefully selected. Their resonance parameters primarily determine suitability for analysis. A first selection can be based on the sensitivity factor defined as follows:[5]

$$S = \frac{g\Gamma_n\Gamma_\gamma}{\Gamma_{\mathrm{tot}}} \frac{a}{E_{\mathrm{res}}^{1-\alpha}}. \tag{14}$$

This is a suitable quantity to compare resonance strengths at different beam energies. In this expression, a is the isotope abundance, g is the statistical spin factor, and α is as defined in Sec. II. In practice, it can be assumed that $1-\alpha \approx 2$. The total neutron width is given by $\Gamma_{\mathrm{tot}}=\Gamma_\gamma+\Gamma_n$ with Γ_γ the capture width and Γ_n the scattering width.

Second, self-shielding determines whether or not a resonance is to be included in analysis. For most objects it is possible to estimate if $d<d_{\mathrm{lim}}$ for a certain resonance. If *a priori* estimations for the density correction factors f_i in Eq. (3) can be made, $\eta(d,E_n)$ can be calculated. If no *a priori* information about the composition of the object is available, an initial analysis using weaker resonances gives an approximation for the factors f_i.

As a third criterion, resonance peaks for which capture is the dominant process, i.e., $\Gamma_\gamma/\Gamma_{\mathrm{tot}}$ is close to 1, are most suitable. For these resonances, the contribution of SC to the total number of recorded capture events is small and can adequately be corrected for as described below. In other words, $Y_{\mathrm{TC,exp}}(E_n) \approx Y_{\mathrm{DC,exp}}(E_n)$ under the lower-energy wing of the capture peak. If, however, $\Gamma_\gamma/\Gamma_{\mathrm{tot}}$ is significantly smaller than 1, scattering is the dominant process for neutrons with energies equal to or close to the resonance energy. These neutrons may be resonance-scattered out of the incoming beam before possibly being captured at lower energies. As a consequence, these capture events disturb the analysis based on DC along the direction of the incoming neutron beam. So, notwithstanding that for these resonances $Y_{\mathrm{TC,exp}}(E_{\mathrm{res}})$ may be high (as is the case, e.g., for 112.2 and 579 eV resonances of ^{116}Sn and ^{65}Cu, respectively), they are not preferable and therefore excluded from DEAP analysis.

In practice, selection of resonances for analysis depends on different parameters as well, mainly related to spectral quality (statistics) and, e.g., local SC contribution to TC and possible overlap with other resonance peaks.

VI. SIMPLE ANALYSIS METHOD

In this section some aspects of DEAP will be considered. This analysis method has been developed for two applications: (i) for determining the elemental composition of irregular objects placed in a wide neutron beam using NRCA and (ii) for 3D imaging of the elemental composition of objects using a narrow neutron beam. In this paper the main attention concerns NRCA.

A. Main characteristics of the analysis method

1. Only a small number of resonance peaks are needed for accurate analysis

As explained in Sec. V, self-shielding influences different recorded resonance peak intensities in different degrees. This feature is key to our analysis method. Assume a series of similar objects made of the same chemical element X and only different in thickness d (in the beam direction). After

TABLE I. Resonances that can be included in DEAP for various elements

Element	Resonance energy (eV)
Cu	230, 402, 650, 807, 994
Sn	38.8, 45.7, 62, 147.9
Sb	6.24, 15.41, 21.4, 29.65
As	47.0, 92.4, 252.7, 455.5
Ag	5.19, 16.3, 30.4, 51.4
Zn	282, 324, 514
In	1.457, 3.85, 9.04
Pb	3063, 3357

NRCA, element X is characterized by n_{res} experimental DC resonance peak intensities $Y_{\mathrm{DC,exp}}(E_{\mathrm{res},i})$ with $E_{\mathrm{res},i}$ the resonance energy for resonance $i=[1,\ldots,n_{\mathrm{res}}]$.

For a very thin object, $Y_{\mathrm{DC,exp}}(E_{\mathrm{res},i})\sim d$ for all n_{res} DC resonance peaks and self-aborption is negligible, i.e., intensity ratios $Y_{\mathrm{DC,exp}}(E_{\mathrm{res},i})/Y_{\mathrm{DC,exp}}(E_{\mathrm{res},j})$ $(i,j=[1,\ldots,n_{\mathrm{res}}])$ are independent of d. If d increases, intensity ratios $Y_{\mathrm{DC,exp}}(E_{\mathrm{res},i})/Y_{\mathrm{DC,exp}}(E_{\mathrm{res},j})$ change values as self-shielding starts to deviate between different DC resonance peaks, making them broader and flatter on the top (see Fig. 4), with all $Y_{\mathrm{DC,exp}}(E_{\mathrm{res},i})$ increasing less and less. The combined DC resonance peak shapes and intensity ratios $Y_{\mathrm{DC,exp}}(E_{\mathrm{res},i})/Y_{\mathrm{DC,exp}}(E_{\mathrm{res},j})$ thus identify a unique value for d. Similarly, for an archaeological object, the resonance peaks of different chemical elements combined allow for determining their individual elemental thicknesses, i.e., the chemical composition of the object. Data fitting requires that $\sigma_c^D(E_n)$, $\sigma_t^D(E_n)$, $R(E_n,E_n')$, and $\varepsilon_{c,\mathrm{rel}}(E_{\mathrm{res}})$ are accurately known for all resonances included in analysis.

Based on analysis results so far, we estimate that two or three resonance peaks per element suffice to determine the chemical composition of an object, provided that $\eta(d,E_{\mathrm{res}})$ is not close to 100% and sufficiently different for these resonances and that baseline and SC counts do not unacceptably impede their analysis (see Sec. VI A 2). It is believed that these conditions can be met for most recorded spectra. The current version of DEAP performs a combined analysis of Cu and one other element which gives the mass ratio of both. Future versions of DEAP will incorporate simultaneous analysis of more than two elements. Table I indicates the resonances that can be included in DEAP for various elements. Spectral quality, SC, and overlapping resonances determine if a resonance is actually used in DEAP.

2. Suitable for all object shapes

The proposed analysis method is not significantly disturbed by SC. As explained before, it will be difficult to adequately and precisely model SC for irregularly shaped objects like archaeological artifacts. In general, this would imply a convolution of probability functions for scattering $P_s(E_{n,0},E_{n,1},d(\psi))$ and that of subsequent capture in the object $P_c(E_{n,1},d'(\theta))$. These functions are similar to Eq. (9) but with dependence of incoming beam angle ψ with respect to the object and neutron path lengths in the object before scattering $d(\psi)$ and between scattering and capture $d'(\theta)$, as illustrated in Fig. 3 for the two-dimensional case.

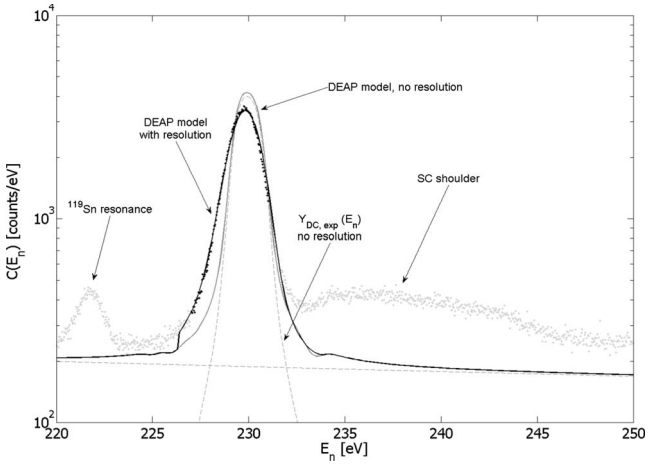

FIG. 6. Comparison between recorded capture counts for a bronze object and DEAP model, illustrating the effect of convolution with resolution function for the 230 eV resonance from ^{65}Cu. Bold data points indicate those included in data fitting.

Both these distributions are strongly dependent on object shape and size, and for objects with irregular shapes, these distributions are not *a priori* known, which seriously hinders quantification of SC. Also, it may well be that the experimental SC yield and the baseline intensity (see further in this section) can hardly be distinguished, furthermore complicating quantification. Even for those object shapes that allow for SC modeling based on an approximate geometric model, data analysis will be seriously slowed down as full spectrum convolution operation must be included in the least-square data fitting algorithm.

We have therefore adopted an approach that is based on avoidance of SC as much as possible. Figure 6 shows part of the NRCA spectrum of the Nijmegen water tap around the resonance energy $E_{\mathrm{res}}=230$ eV from ^{65}Cu. The SC shoulder is clearly visible for energies just above the resonance energy. Only bold data points have been selected for data analysis.

The left wing of the resonance capture peak is not significantly disturbed by the SC spectrum (see Sec. IV) and is suitable for data fitting based on Eq. (5). The energy range is limited on the low energy side of the 230 eV resonance peak by the presence of a ^{119}Sn resonance at 222.6 eV: overlapping resonances should best be avoided as data analysis becomes unnecessarily complicated. On the low-energy side, only those data points for which the contribution of SC to $Y_{\mathrm{TC,exp}}(E_n)$ is small and often negligible are selected, while a minimum number of data points on the high-energy side of the resonance peak is required for accurate determination of the peak energy value. Together, these selected data points sufficiently satisfy Eq. (5). The systematic uncertainty related to the selection of data points in windows around the resonances is discussed in Sec. VI B. At resonance energies below 20 eV, the fraction of SC underneath a resonance peak becomes larger and DEAP applies correction for SC based on GEANT4 simulations, as discussed in Sec. VI B.

3. Based on availability of cross sections for neutron capture and total attenuation

Pointwise Doppler-broadened cross sections can be accessed in standardized data formats through, e.g., the JANIS (Java-based Nuclear Information Software) display program,[17] containing the latest evaluated data libraries, such as JEFF-3.1, ENDF/B-VII, JENDL-3.3, etc. The quality of these cross sections primarily determines the accuracy of the analysis with DEAP, to which they are directly fed.

4. Fast data analysis through efficient convolution at resonance energies only

Since the shape and intensity of the recorded resonance capture peaks are determined not only by Doppler broadening but also by the neutron energy resolution function $R_E(E_n, E_n')$, the latter must be included in the analysis. For GELINA the neutron energy resolution function is well known.[18] As the analytical model is based on fitting line shapes of a limited number of selected resonance peaks, it is sufficient to perform convolution only with $R_E(E_n=E_{\mathrm{res}}, E_n')$ rather than full spectrum convolution, as such speeding up data analysis. Figure 2 clearly illustrates the effect of convolution with $R_E(E_n=E_{\mathrm{res}}, E_n')$ on the resonance peak shape.

5. Relative detection efficiencies determined with calibration measurements

As the number of γ-rays emitted after neutron capture and their energies vary between different isotopes and are not *a priori* known, calibration measurements are needed to quantify differences in isotope dependent detection efficiencies. Calibration samples are usually metal alloys or sandwiches of metal foils with well-defined elemental compositions and should be measured in the same experimental setup as the archaeological object. In the analysis of objects spectra, DEAP accounts for the above mentioned differences by including $\varepsilon_{c,\mathrm{rel}}(E_{\mathrm{res}})$, i.e., relative detection efficiencies for E_{res}, which are derived from prior fits to the calibration spectra. γ-ray interactions inside the sample are not taken into account.

6. Semiempirical model for baseline intensity

As can be seen in Fig. 1, the recorded capture spectrum consists of resonance peaks on top of a "baseline" (BL) intensity. These baseline counts originate from SC in the object, experimental setup, and direct surroundings. Rather than detailed modeling of complete experimental circumstances that in principle enables quantification of SC, we choose a more pragmatic (semiempirical) approach. Outside the resonances, potential scattering is the dominant neutron interaction process. The potential scattering cross section σ_{pot} is in good approximation constant for all elements and therefore gives an energy-independent reduction of the count rate. The effective cross section $\sigma_{\mathrm{SC,eff}}(E_n)$ for SC can therefore be described by

$$\sigma_{\mathrm{SC,eff}}(E_n) \propto \sigma_{\mathrm{C,eff}}(E_n), \tag{15}$$

i.e., $\sigma_{\mathrm{SC,eff}}(E_n)$ has approximately the same energy dependence as an effective capture cross section $\sigma_{\mathrm{C,eff}}(E_n)$ accounting for the contributions of all elements in the object. Therefore, $\sigma_{\mathrm{SC,eff}}(E_n)$ can be parametrized as

$$\sigma_{\mathrm{SC,eff}}(E_n) = p(2) \cdot E_n^{p(3)}. \tag{16}$$

During data analysis the fitting parameter $p(2)$ acts as a normalization constant, and fitting parameter $p(3)$ as the energy dependence of $\sigma_{\mathrm{SC,eff}}(E_n)$, the value of which approaches -0.5 when $E_n \to 0$. This is known as the $1/\nu$ law that can be derived from the Breit–Wigner formula for slow neutron capture cross sections, which holds for nearly all nuclei.[19]

The baseline capture intensity $\mathrm{BL}(E_n)$ as a function of incoming neutron energy E_n can then be modeled as follows:

$$\mathrm{BL}(E_n) = \varphi_0(E_n) \cdot \sigma_{\mathrm{SC,eff}}(E_n). \tag{17}$$

7. Quick analysis and ease of use

The data fitting in our software package is performed by MFIT (Version 4.2),[20] an application for interactive nonlinear fitting, in our case running under MATLAB Version 7.5.0 R2007b.[21] MFIT provides a fast, easy, flexible, and powerful way of fitting arbitrary model functions to two-dimensional (i.e., x-y) data and has the additional advantage that large amounts of spectra can be analyzed in batches.

In the analysis we use the Nelder–Mead least-square fitting algorithm with a limited number of six free fitting parameters to derive elemental mass fractions. Additional (trivial) free fitting parameters are used to perform fine-tuning of the exact resonance peak energies and, in the case of calibration samples (analyzed prior to the object), to account for relative detection efficiencies. The user provides input via an Excel input file containing experimental parameters such as the neutron flight path length, the elements to be analyzed, and the neutron beam filter materials and thicknesses. The DEAP Excel output file provides the user with elemental mass ratios and thicknesses and derived overall composition of the object analyzed.

B. Results from DEAP for the Nijmegen water tap

The analytical model used to approximate $Y_{\mathrm{TC,exp}}(E_n)$ is given by

$$Y_{\mathrm{TC,exp}}(E_n) \cong K_1 \sum_{i=1}^{n_{\mathrm{res}}} \left[\int_{\mathrm{res},i} R_E(E_{\mathrm{res},i}, E_n') \times \{\varepsilon_{c,\mathrm{rel}}(E_{\mathrm{res},i}) \varphi(E_n') Y_{\mathrm{DC}}(E_n', \langle d \rangle)\} dE_n' \right] + \mathrm{BL}(E_n), \tag{18}$$

i.e., the sum of n_{res} experimental DC capture yields $Y_{\mathrm{DC,exp}}(E_n)$ around respective resonance energies $E_{\mathrm{res},i}$ plus a term accounting for baseline intensity, with K_1 a normalization factor that is one of the fit parameters, as is the mean object thickness $\langle d \rangle$ in the direction of the incoming neutron beam [cf. Eq. (5)].

Figure 1 shows experimental data from the NRCA experiment with the Nijmegen water tap together with results from the DEAP analysis for Cu and Ag. Similar analysis has been performed for other elements in the water tap. The re-

TABLE II. Results from DEAP analysis for the Nijmegen water tap, compared with those from Schut *et al.* (Ref. 9). The error in wt % are compounded from those on the mass ratios.

Elemental mass ratios	DEAP analysis	Schut *et al.*	Element	wt % (DEAP)
			Cu	74.52 ± 1.50
Pb/Cu	0.217 ± 0.027	0.212 ± 0.031	Pb	16.15 ± 1.99
Sn/Cu	0.1106 ± 0.0043	0.1114 ± 0.0038	Sn	8.24 ± 0.36
Zn/Cu	0.0118 ± 0.0007	0.0120 ± 0.0005	Zn	0.878 ± 0.052
Sb/Cu	0.001 38 ± 0.00015	0.001 59 ± 0.00005	Sb	0.103 ± 0.011
Ag/Cu	0.000 62 ± 0.00010	0.000 72 ± 0.00003	Ag	0.046 ± 0.007
As/Cu	0.000 80 ± 0.00004	0.000 75 ± 0.00003	As	0.060 ± 0.003

sults are given in Table II as mass ratios relative to Cu and the corresponding elemental composition of the Nijmegen water tap. The mass ratios are compared to those from Schut *et al.*[9] The total errors in Table II follow from statistical fluctuations in recorded data and a systematic uncertainty related to the selection of data points in windows around the resonances, accuracy of baseline intensity, cross sections, and experimental resolution. By choosing different widths and positions of the selection windows around the resonance energies, e.g., a systematic error of 0.0024 was found for the mass ratio Sn/Cu=0.1106. The influence of baseline intensity was studied by applying a 10% variation around the value derived from data fitting. From this we find a systematic error of 0.0019, adding up to a total value of 0.0043 (i.e., a relative error value of 3.9%). In addition there is, for the low-energy resonances below about 20 eV, an extra uncertainty related to the correction for SC in DEAP (further in this section), which explains the higher relative errors for Sb and Ag.

Agreement between both methods is excellent, with elemental mass ratios equal within the error bars. The Ag/Cu and Sb/Cu mass ratios from DEAP are somewhat lower than the values found by Schut *et al.*[9] This is believed to be caused by different treatments of SC contribution by both methods, especially for low resonance energies.

A first indication of the contribution of SC for low resonance energies was provided by a GEANT4 simulation for a neutron beam (GELINA fluence rate) irradiating a 10 mm thick bronze (about 88.1 and 11.5 wt % for Cu and Sn, respectively) plate containing some of the trace elements also found in the Nijmegen water tap, namely, Ag, As, and Sb (adding up to about 0.5 wt %). For the 5.19 eV Ag resonance, e.g., different contributions to TC are shown in Fig. 7. Since the SSC spectrum partly overlaps with the DC resonance peak, the relative SC intensity under the low-energy wing of the resonance peak is significant compared to higher resonance energies. The assumption $Y_{\mathrm{TC,exp}}(E_n) \cong Y_{\mathrm{DC,exp}}(E_n)$ does not hold anymore and, without correction, DEAP would overestimate the mass ratio for Ag based on this resonance. One way to estimate the SC counts under low-energy resonances is by using a parametric fitting technique assuming Gaussian SC distributions, as was done by Schut *et al.*[9] This approach provides an approximate correction, but is in some cases hindered by overlapping DC and SC contributions and does not work very well when these

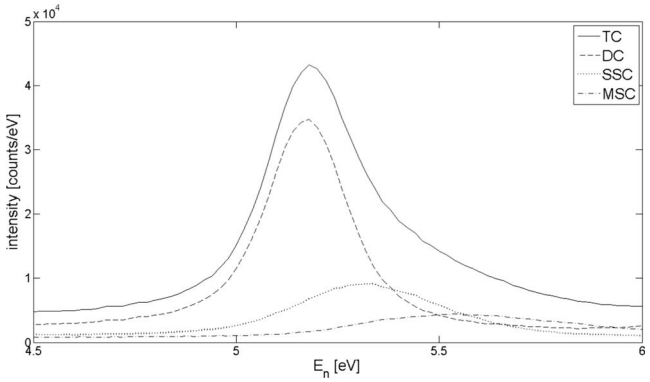

FIG. 7. Different contributions to TC for the 5.19 eV Ag resonance as quantified by a GEANT4 simulation for a neutron beam (GELINA fluence rate) irradiating a 10 mm thick bronze plate containing Ag as a trace element.

can no longer be distinguished in the recorded spectrum. We have therefore performed similar simulations for plate thicknesses of 0.5, 1, 3, 5 and 10 mm (i.e., a total range between about 0.4 and 8 g cm^{-2} Cu) to derive overall correction factors for DEAP for SC at low resonance energies (see Fig. 8). For thicker objects, these values are extrapolated in DEAP to give SC correction factors valid up to about 12 g cm^{-2} Cu. The correction factors have been derived by comparing mass ratios from DEAP analysis on the DC and TC signals separately recorded in the simulations. The correction factors are largely determined by the lowest energy resonance included in analysis (e.g., 5.19 eV for Ag and 15.41 eV for Sb), i.e., the inclusion of higher resonance energies does not significantly change the correction factor for that element. Correction for SC is substantial for In (lowest resonance energy of 1.46 eV) and Ag (5.19 eV) and dependent on object thickness for Sb (15.41 eV). As the overlap between SC and DC becomes less with increasing energy, SC does not significantly influence DEAP results for resonance energies above about 20 eV. The SC correction for Sn is therefore only about 2% at 8 g cm^{-2} Cu. The influence of object composition on SC correction factors has been assessed by rerunning

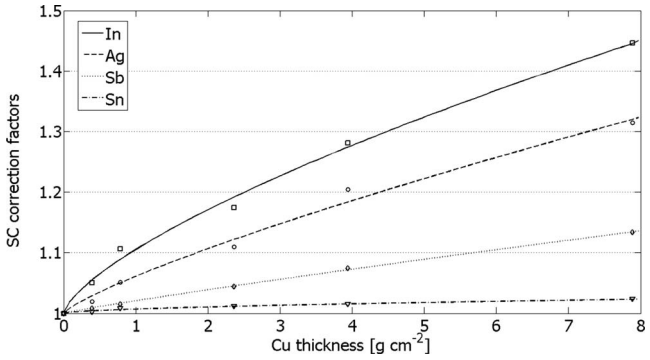

FIG. 8. Correction factors for SC for elements with low-energy resonances as a function of Cu thickness, derived from GEANT4 simulations for a neutron beam (GELINA fluence rate) irradiating a bronze plate with thicknesses of 0.5, 1, 3, 5, and 10 mm (i.e., between about 0.4 and 8 g cm^{-2} Cu), containing those trace elements indicated in the figure legend. The correction factor is found by comparing mass ratios from DEAP analysis on the DC and TC signals separately recorded in the simulations. The data points indicate simulation results for the different plate thicknesses. The fitted lines are used for smoothing and are applied in DEAP where they are extrapolated for thicker objects to give SC correction factors valid up to about 12 g cm^{-2} Cu.

the 8 g cm^{-2} Cu simulation with the same object but also containing 15 wt % lead (i.e., about 74.9, 9.8, and 15 wt % for Cu, Sn, and Pb, respectively). The influence is found to be negligible as SC structures are predominantly determined by scattering on Cu atoms (main component) with DC/TC ratios for both runs equal within 0.5%.

Values for Pb show a high relative error of about 12% for both methods mainly due to poor statistics for Pb resonances in the energy region around 3 keV, where neutron flux intensity is low. As a consequence, the Cu wt % also shows relatively large errors. The Fe/Cu ratio as reported by Schut *et al.*[9] has not been analyzed with DEAP since the 1149 eV resonance from ^{56}Fe is now believed to overlap with the 1150 eV resonance from ^{119}Sn. This severely hinders the determination of the Fe wt %, which is therefore ignored. The composition of the Nijmegen water tap as quoted in the last column of Table II is thus based on listed DEAP analyzed elements only. The Cu thickness is best determined from the analysis of Cu in combination with major components in the object. Since the Cu thickness is needed to correct for SC, the major components must be analyzed prior to the minor ones. Taking the average from the analysis for Cu/Sn and Cu/Pb, a Cu thickness of 7.3 ± 0.4 g cm^{-2} is found, which agrees well with the value of 7.2 ± 0.8 g cm^{-2} found by Schut *et al.*[9]

VII. DISCUSSION AND CONCLUSIONS

Good agreement has been found between results from the new DEAP composition analysis method and results reported by Schut *et al.*[9] and Amkreutz *et al.*[11] concerning two ancient bronze artifacts both containing a number of minor elements. The achieved accuracy is sufficient for archaeological purposes.

DEAP is a software package which can automatically and quickly analyze multiple NRCA spectra in a relatively simple way, yielding the elemental composition of objects, largely independent of their shapes and sizes. Rather than detailed modeling of SC, which is difficult for irregularly shaped objects, DEAP has adopted an analysis approach based on avoidance of SC. The errors due to this approach are expected to be small although increasing with decreasing resonance energies. DEAP uses an approach similar to that of the double-ratio method[1] by comparing a (small) set of resonances of the object with those of a calibration sample, but with correction for self-shielding included and with a fully automated fitting procedure. Application of DEAP is not restricted to bronze objects but can be extended to objects containing elements with resonances in the epithermal neutron energy range. DEAP reads in raw histogram data, performs all data correction (e.g., dead-time correction), data reduction, and conversion steps and outputs elemental mass ratios and thicknesses and derived overall composition of the object analyzed.

DEAP will also be used in the framework of the Ancient Charm[7] project as data analysis program for NRCI experiments. NRCI provides 3D visualization and elemental quantification of the internal structure of archaeological objects by performing scanning measurements with a collimated neutron beam on objects in computed tomography based experimental setups. The hundreds to thousands of short runs are in the order of several minutes, each run producing a neutron resonance spectrum which should be analyzed during the NRCI experiment in a fully automated way.

DEAP is freeware and will be made available for downloading through the Ancient Charm[7] website.

ACKNOWLEDGMENTS

We would like to thank P. Schillebeeckx, A. Borella, and R. Wynants for the ongoing collaboration in NRCA experiments at GELINA and in the framework of the Ancient Charm project. We thank F. Gunsing for providing us with GELINA resolution function data. We are grateful to W. Mondelaers and his staff for the dedicated and skillful running of the GELINA facility of the Joint Research Centre, IRMM, in Geel. This study has been carried out as part of the EU FP6 Ancient Charm project, funded by the European Commission under Contract No. 15311.

[1] H. Postma, M. Blaauw, P. Bode, P. Mutti, F. Corvi, and P. Siegler, J. Radioanal. Nucl. Chem. **248**(1), 115 (2001).
[2] M. Blaauw, H. Postma, and P. Mutti, Nucl. Instrum. Methods Phys. Res. A **505**, 508 (2003).
[3] H. Postma, P. Schillebeeckx, and R. B. Halbertsma, Archaeometry **46**(4), 635 (2004).
[4] M. Blaauw, H. Postma, and P. Mutti, Appl. Radiat. Isot. **62**, 429 (2005).
[5] H. Postma and P. Schillebeeckx, J. Radioanal. Nucl. Chem. **265**(2), 297 (2005).
[6] H. Postma, J. J. Butler, P. Schillebeeckx, and C. W. E. van Eijk, Nuovo Cimento Soc. Ital. Fis., C **30**, 105 (2007).
[7] G. Gorini, Nuovo Cimento Soc. Ital. Fis., C **30**, 47 (2007). EU FP6 Ancient Charm project under Contract No. 15311 (http://ancient-charm.neutron-eu.net/ach).
[8] M. C. Moxon, T. C. Ware, and C. J. Dean, REFIT-2007, A least-square fitting program for resonance analysis of neutron transmission, capture, fission and scattering data, Users Guide for REFIT-2007-08, UKNSF, 2007, p. 216.
[9] P. A. C. Schut, W. Kockelmann, H. Postma, D. Visser, P. Schillebeeckx, and R. Wynants, J. Radioanal. Nucl. Chem. **278**, 151 (2008).
[10] A. Borella, Determination of the neutron resonance parameters for ^{206}Pb and of the thermal neutron capture cross section for ^{206}Pb and ^{209}Bi, Ph.D. thesis, Institute of Reference Materials and Measurements, 2005, p. 59.
[11] L. Amkreutz, A. Borella, M. Clarijs, D. Fontijn, H. Kamermans, W. Kockelmann, A. Paradowska, H. Postma, P. Schillebeeckx, and D. Visser, The Buggenum sword studied at the GELINA facility (to be submitted).
[12] A. Borella, G. Aerts, F. Gunsing, M. Moxon, P. Schillebeeckx, and R. Wynants, Nucl. Instrum. Methods Phys. Res. A **577**, 626 (2007).
[13] G. F. Knoll, *Radiation Detection and Measurement* (Wiley, New York, 2000).
[14] H. Postma, M. C. Clarijs, V. R. Bom, and C. W. E. van Eijk, Some aspects concerning neutron resonance capture analysis and imaging, AC Report No. AC-06-IR02, 2006.
[15] N. M. Larson and K. N. Volev, Validation of Multiple-Scattering Corrections in the Analysis Code SAMMY. PHYSOR, 2002.
[16] See GEANT4 web site at http://geant4.cern.ch.
[17] N. Soppera, M. Bossant, H. Henriksson, P. Nagel, Y. Rugama, International Conference on Nuclear Data for Science and Technology, 2007 (unpublished).
[18] M. Flasška, A compact fast-neutron producing target for high resolution cross section measurements, Ph.D. thesis, Delft University of Technology, 2006.
[19] K. H. Beckurts and K. Wirtz, *Neutron Physics* (Springer-Verlag, Berlin, 1964).
[20] MFIT interactive nonlinear fitting and data analysis program (http://wwwold.ill.fr/Computing/resources/software/matlab/doc/mfit4/).
[21] MATLAB is a product from The MathWorks (http://www.mathworks.com/products/matlab).